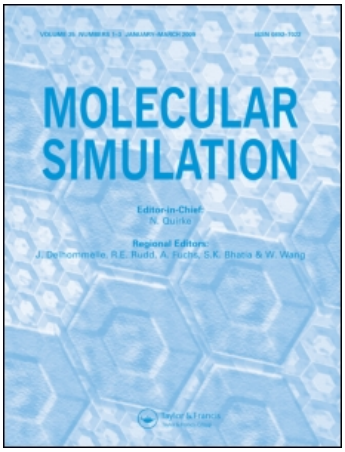

Molecular Simulation
Publication details, including instructions for authors and subscription information:
http://www.informaworld.com/smpp/title~content=t713644482

Molecular dynamics simulation of the kinetic sintering of Ni and Al nanoparticles

Brian J. Henz[a]; Takumi Hawa[bc]; Michael Zachariah[bc]
[a] Advanced Computing and Computational Sciences Division, U.S. Army Research Laboratory, ATTN: AMSRD-ARL-CI-HC, Aberdeen Proving Ground, Aberdeen, MD, USA [b] National Institute of Standards and Technology, Gaithersburg, MD, USA [c] Department of Mechanical Engineering and the Department of Chemistry and Biochemistry, University of Maryland, College Park, MD, USA

To cite this Article Henz, Brian J. , Hawa, Takumi and Zachariah, Michael(2009) 'Molecular dynamics simulation of the kinetic sintering of Ni and Al nanoparticles', Molecular Simulation, 35: 10, 804 — 811
To link to this Article: DOI: 10.1080/08927020902818021
URL: http://dx.doi.org/10.1080/08927020902818021

Molecular Simulation
Vol. 35, Nos. 10–11, September 2009, 804–811

Taylor & Francis
Taylor & Francis Group

Molecular dynamics simulation of the kinetic sintering of Ni and Al nanoparticles

Brian J. Henz[a]*, Takumi Hawa[bc1] and Michael Zachariah[bc]

[a]*Advanced Computing and Computational Sciences Division, U.S. Army Research Laboratory, ATTN: AMSRD-ARL-CI-HC, Aberdeen Proving Ground, Aberdeen, MD 21005, USA;* [b]*National Institute of Standards and Technology, Gaithersburg, MD, USA;* [c]*Department of Mechanical Engineering and the Department of Chemistry and Biochemistry, University of Maryland, College Park, MD, USA*

(*Received 22 December 2008; final version received 6 February 2009*)

The kinetic sintering of Ni and Al nanoparticles is considered using molecular dynamics simulations. We report on the effects of nanoparticle size on sintering temperature and time, with results showing that surface energy has a slight effect on both results. The effect of surface energy on combustion temperature is limited to nanoparticles of less than 10 nm in diameter. An analysis of the various alloys formed during sintering gives insight into the reaction process. The formation of Al-rich compounds is observed initially with a final equilibration and rapid formation of the eutectic alloy immediately preceded by melting of the Ni nanoparticle. We have observed that nanoparticle size and surface energy are both important factors in determining the adiabatic reaction temperature for this material system at nanoparticle sizes of less than 10 nm in diameter.

Keywords: sintering; SHS reaction; nanoparticle

1. Introduction

Nanoparticles have interesting physical properties that often vary from the bulk material. Some of these properties, including increased reactivity [1], are due to the high surface area to volume ratio of nanoparticles. With this in mind nanoparticles may provide enhanced energy release rates for explosive and propellant reactions [2].

The self-propagating high-temperature synthesis (SHS) reaction of intermetallic compounds releases energy [3] during alloy formation. In addition to the energetic reaction observed in the laboratory with these materials it is possible to produce structural components that contain this energy release property. Once ignited, the SHS reaction releases a large amount of energy in a short period of time. One significant difference between SHS and typical combustion processes is that the reactants and products are confined to the condensed state [4]. The SHS process has many potential applications where heat generation is required and oxygen is not available or gaseous products are not desirable. These include alloy formation, net-shape processing, propellants, and as initiators. One of the compounds formed from the SHS reaction, and studied here, is NiAl or nickel aluminide. NiAl is an important alloy because of its desirable high temperature strength and oxidation resistance [5] and the high energy of formation [6]. Recently, Weihs and co-workers [7] have also used NiAl nanolaminate systems in applications of reactive welding.

Not surprisingly, since the reaction involves solid starting materials, particle size has a significant effect on the properties of the reaction product and the SHS reaction itself [8]. The simulation and analysis of nanoparticle coalescence without the SHS reaction for like materials is extensive [9–14] and involves surface passivation [10], size differences [9,11], and phase change [9] considerations. The analyses here include all of the previously listed concerns with an additional energy release term from the heat of formation.

The primary focus of this paper is to use atomistic simulation to model the SHS reaction that occurs during the sintering of Ni and Al nanoparticles. Fortunately, there have been numerous efforts to determine accurate empirical potentials for simulating the Ni–Al material system [15]. Prior simulations using these potentials have investigated the diffusion of Ni and Al atoms [15], point-defect concentrations in NiAl [16], and plasticity [17] in addition to many other mechanical and chemical properties. These efforts have primarily focused on bulk materials rather than nanoparticle systems [18], even though there are many manufacturing processes that produce nanometre sized powders for SHS reactions [19]. For this simulation effort we have chosen a set of embedded atom method (EAM) parameters that reproduce reasonably well the properties of Ni, Al, and NiAl in the temperature range of interest.

2. Simulation approach

In this work we employ classical molecular dynamics (MD) with an EAM interatomic potential to study the reactive

*Corresponding author. Email: brian.j.henz@us.army.mil

ISSN 0892-7022 print/ISSN 1029-0435 online

DOI: 10.1080/08927020902818021
http://www.informaworld.com

sintering process. The EAM is used because of its accuracy and capability to scale up to material systems with over 10^6 atoms. The MD simulations are compared with thermodynamic analyses in order to provide validation of the simulation results and assess the expected energy release.

These MD simulations were conducted using the LAMMPS software package [20]. For the Ni–Al interactions the Finnis-Sinclair EAM potential [21] from Angelo et al. [22] was used. The Finnis-Sinclair EAM potential allows for non-symmetric embedding potential terms, potentially providing improved accuracy for metallic alloys [23]. In addition, to the parameters for NiAl from Angelo et al. other authors have also developed parameters for the Ni–Al system [16] that may also be described by using the Finnis-Sinclair EAM.

Three primary nanoparticle sizes considered in this work from smallest to largest are nanoparticles with 1289, 5635, and 36,523 atoms each, which correspond approximately to Al nanoparticles with diameters of 3, 5 and 10 nm, respectively. Throughout this work, references to nanoparticle size correspond to the Al nanoparticle with the understanding that all simulations are performed with atomic ratios of 1:1. This range of sizes was chosen because it represents nanoparticles that may be produced in the laboratory, and which requires reasonable computational time to conduct parametric studies. For the largest system considered, namely the 10 nm diameter nanoparticle with 73,046 atoms, a kinetic reaction simulation requires approximately 48 h and 64 processor cores to complete a few nanoseconds of simulated time using 3.0 GHz Intel Woodcrest processors with LAMMPS.

3. Thermodynamic analysis of separate nanoparticles

In a previous effort by these authors [24] a more detailed thermodynamic analysis is presented with the highlights covered here. The separate nanoparticle system is used as a model for powder metallurgy systems where Ni and Al particles are compressed into a structural component. A thermodynamic analysis of the sintering of separate Ni and Al nanoparticles is used here to determine the expected trends and data points for simulation validation. In the thermodynamic analysis we are interested in determining the system parameters of the Ni–Al nanoparticle system that contribute to the combustion temperature and reaction time. Here, we have assumed an adiabatic process so that energy released to the surroundings can be ignored. This is a good approximation since the reaction occurs on relatively short time scales and in addition the nanoparticles are expected to be included in a much larger system where the overall surface to volume ratio is small, limiting convective and radiative heat loss. The SHS reaction of an equimolar Ni and Al mixture is written as:

$$0.5\mathrm{Ni} + 0.5\mathrm{Al} \rightarrow \mathrm{Ni}_{0.5}\mathrm{Al}_{0.5}. \quad (1)$$

In order to compute the adiabatic temperature for the synthesis reaction the enthalpy of the products and reactants must be equal

$$H_{\mathrm{prod}}(T_{\mathrm{ad}}) = H_{\mathrm{reac}}(T_0). \quad (2)$$

Assuming that the reaction begins with the reactants at 600 K, above the simulated melting temperature of the Al nanoparticles, the enthalpy of the reactants is computed as,

$$H_{\mathrm{reac}} = (0.5)(H_{\mathrm{Al,fusion}}) + (0.5)(H_{\mathrm{Al,600\,K}} + H_{\mathrm{Ni,600\,K}}) = 11.85\,\mathrm{kJ/mol}. \quad (3)$$

This enthalpy result includes the enthalpy of solid Ni and liquid Al [6]. The Al nanoparticle is assumed to be liquid because for small nanoparticles the melting temperature is known to be appreciably below the bulk melting temperature [25]. Additionally, for the EAM potential used here [22] the aluminium is liquid for these nanoparticle sizes at 600 K. The choice of initial temperature will have a nearly linear effect on the adiabatic temperature as long as the initial temperature is between the melting point of the Al and Ni nanoparticles. This linear effect has been observed in experiments [26], and is a reasonable assumption so long as the heat capacities of the solid phases of Ni and NiAl are relatively insensitive to temperature in the ranges studied.

For the products of the sintering process the enthalpy calculation must take into account contributions from the melting of the nickel and the NiAl nanoparticle, enthalpy of formation for the NiAl alloy, and changes in surface energy.

The last contribution to the enthalpy of the products, results from the change in surface energy, and is due to the reduced total surface area of the combined nanoparticle [27]. The contribution to the change in system energy from the drop in surface area is given as Equation (4)

$$\Delta E_{\mathrm{surf}} = \sigma_{\mathrm{NiAl}} \cdot a_{\mathrm{NiAl}} - (\sigma_{\mathrm{Ni}} \cdot a_{\mathrm{Ni}} + \sigma_{\mathrm{Al}} \cdot a_{\mathrm{Al}}). \quad (4)$$

In Equation (4) a_{NiAl}, a_{Ni}, and a_{Al} are the surface areas of the NiAl, Ni, and Al nanoparticles, respectively. The approximate change in system energy from surface tension versus nanoparticle size is tabulated in Table 1.

Table 1. Total change in system surface energy versus nanoparticle size.

Nanoparticle radius (nm)	ΔE_{surf} (kJ/mol)
3	−18.35
5	−11.41
10	−6.17

In Table 1 the apparent trend is for a lower surface energy contribution to the sintering process as the nanoparticle size increases. Intuitively, one may expect this because the surface area to volume ratio is also decreasing with increasing particle size, and therefore has less influence on the sintering process. With the enthalpy of formation for NiAl measured at approximately −65 kJ/mol [28,29] the surface energy contribution to the change in enthalpy for coalescence of 10 nm diameter nanoparticles is less than 10% of the total enthalpy change. This means that even at relatively small nanoparticle sizes, e.g. 10 nm, the effect of nanoparticle size on energy release is minimal.

Following the preceding discussion it is now possible to take into account many of the sources of enthalpy change in the reaction products including phase and surface area changes. The enthalpy of the products is now estimated as

$$H_{\text{prod}} = H_{\text{form,NiAl}} + \Delta H_{\text{surf}} + \int_{298\,\text{K}}^{T_{\text{ad}}} C_{p,\text{NiAl}}(T)\mathrm{d}T + H_{\text{melt,Ni}}. \quad (5)$$

The heat capacity for solid and liquid NiAl is given in Kubaschewski et al. [21]. For the 3 nm case, assuming the NiAl nanoparticle melting temperature to be about 1350 K, or the simulated melting point of a similarly sized Ni nanoparticle it is possible to compute the adiabatic reaction temperature, Table 2. The choice of melting temperature for NiAl has little effect on the results so long as the melting temperature is reached and the NiAl material is liquid during the sintering process. The bulk melting temperature for NiAl is 1658 K, but size effects and EAM potential accuracy limit the computed melting temperature during MD simulations. Based on the results in Table 2 a higher melting temperature would only affect sintering of the bulk material or nanoparticles over 10 nm in diameter but this size range was outside of the simulation efforts here.

In the Section 2 we will observe that these results are reasonable and accurately predict the simulated increase in temperature attributable to the contribution from the surface energy.

Table 2. Computed adiabatic temperature versus nanoparticle radius for the three nanoparticles sizes studied.

Nanoparticle radius (nm)	T_{ad} (K)
3	2115
5	1920
10	1772
∞	1599

For completeness the thermodynamic results for the contact of flat surfaces or infinitely sized spheres, where the change in surface energy is insignificant, is appended.

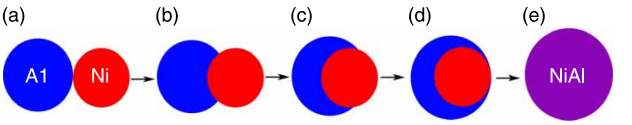

Figure 1. Illustration of sintering process showing liquid Al nanoparticle first coating the solid Ni nanoparticle and then complete alloying after the Ni nanoparticle has melted.

4. The coalescence processes

The sintering process for Ni and Al nanoparticles consists of two processes, namely coalescence and alloying. In this work we have considered the coalescence of a two nanoparticle system with an Al and an Ni nanoparticle with an atomic ratio of unity. A complete reaction of this system will result in a single NiAl nanoparticle. The MD simulations considered use adiabatic conditions with a constant number of atoms and conserved system energy (NVE). The purpose of these simulations is to analyse the effect of nanoparticle size on sintering time, adiabatic combustion temperature, solution formation, and visualisation of the combustion process. The assumed process is illustrated in Figure 1.

In Figure 1 the nanoparticles are initially in contact at a point (a) and the Al nanoparticle is larger than the Ni nanoparticle because of the longer Al—Al bond length. The MD simulations are initialised at 600 K so that the Al nanoparticle is liquid and the Ni nanoparticle is solid. In Figure 1 the sintering process proceeds with the liquid Al nanoparticle initially coating the solid Ni nanoparticle while forming some Ni—Al bonds at the interface (b–d). Next, the alloying process proceeds with the Ni nanoparticle being heated above its melting point and becoming liquid so that rapid atomic mixing may occur (e). The formation of Ni—Al bonds beyond the interfacial surface requires additional mixing of Ni and Al atoms. The most likely route for this process is the diffusion of interfacial Ni atoms into the liquid Al. Once the temperature of the system reaches the melting point of the Ni core the rate of mixing will increase considerably as will the energy conversion from the heat of formation.

The nanoparticle sintering process is driven by two sources of energy as previously discussed. The first of these is a decrease in surface area that lowers the total surface energy of the system. This energy release mechanism is also observed in the sintering of homogeneous material systems such as silicon nanoparticles [27,30]. In Figure 1(d) the Ni nanoparticle is fully coated and only the Al is exposed to the atmosphere, but as the sintering process proceeds the surface energy continues to drop as Ni atoms reach the system surface. The second, and more significant, source of energy change is from the reactive synthesis that occurs initially at the interface between the nanoparticles and later throughout the entire system as atomic mixing proceeds. The energy

release from the surface sintering is proportional to the surface area of the Ni nanoparticle that is coated by Al and eventually in the whole system to the total number of Ni and Al atoms. Finally, with the temperature increase there is a decrease in the viscosity of the liquid aluminium that will affect the predicted coalescence time.

The coalescence of nanoparticles in the liquid and solid phases has been examined extensively [9–11]. These studies are primarily concerned with the coalescence of two liquid or two solid nanoparticles. The analysis for the Ni–Al system requires considering the coalescence of a liquid Al nanoparticle and a solid Ni nanoparticle. The coalescence of a single liquid and single solid gold nanoparticle has previously been considered by Lewis et al. [9]. This analysis is similar to the situation here except that the material system considered was homogeneous, whereas we are concerned with a heterogeneous material system.

In Lewis et al. [9] the author was able to simulate two phases occurring simultaneously for a single material by choosing the size of each nanoparticle such that at a specific temperature the phase of the nanoparticles is different. Lewis found that the coalescence process proceeded in two stages, first the contact area was maximised and second 'sphericization' took place driven by surface diffusion. The first stage is much faster than the second and is very similar to the process observed here, where the Al nanoparticle maximises the contact area and partially coats the Ni nanoparticle. In this case there is an added driving force in addition to the surface energy, specifically the energy release upon the preferential formation of Ni—Al bonds which are at a lower energy state than the existing Al—Al and Ni—Ni bonds. During the second stage the atoms in the two nanoparticles diffuse and rearrange until the system becomes a single spherical nanoparticle. This stage is driven strongly by the formation of Ni—Al bonds and is expected to occur on a much shorter time scale than for two nanoparticles of the same material. The MD simulation results shown in the following section will explore this assumption.

5. MD simulation results of nanoparticle sintering

In this section the MD simulation results for the sintering of Ni and Al nanoparticles is presented and discussed. The simulation results include the computed adiabatic sintering temperature, sintering time, process visualisation, and analysis of the temporal and spatial distribution of solutions formed during sintering.

In Figure 2 each of the steps in the coalescence process is illustrated with plots from an MD simulation of the coalescence of 10 nm diameter Al and Ni nanoparticles. The correlation of the sintering stages to the reaction temperature and time for the same system is plotted

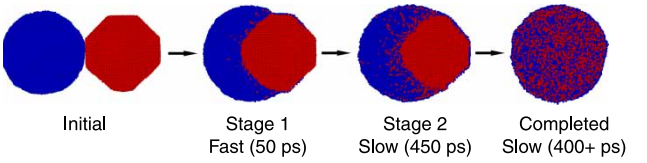

Figure 2. Cross sectional view from MD simulations of Ni/Al nanoparticle sintering process showing the start of the second stage of coalescence, where diffusion is the driving force as opposed to contact area maximisation. Aluminium atoms are blue and Nickel atoms are red.

in Figure 3. In the initial step the liquid Al nanoparticle, blue atoms in Figure 2, has melted and is spherical in shape. The solid Ni nanoparticle, red atoms, has large faceted sides and is a single crystal; a typical configuration for a crystalline nanoparticle at low temperatures. During stage 1 the Al nanoparticle is attracted to the Ni surface because of the dual driving forces of surface energy minimisation and Ni—Al bond formation. This period lasts about 50 ps in this simulation as noted in Figures 2 and 3. Between stages 1 and 2 the driving forces associated with the surface energy are counteracted by a resistance to flow in the Al nanoparticle, causing the coalescence process to slow down dramatically. During stage 2, lasting about 450 ps, the surface area is not changing although the chemistry is shifting from an Al-rich compound to a more eutectic NiAl compound. As only the chemistry of the exposed surface is changing the surface energy release rate drops considerably. The subsequent energy release is almost entirely attributable to the formation of Ni—Al bonds. This stage lasts a much longer time than the initial

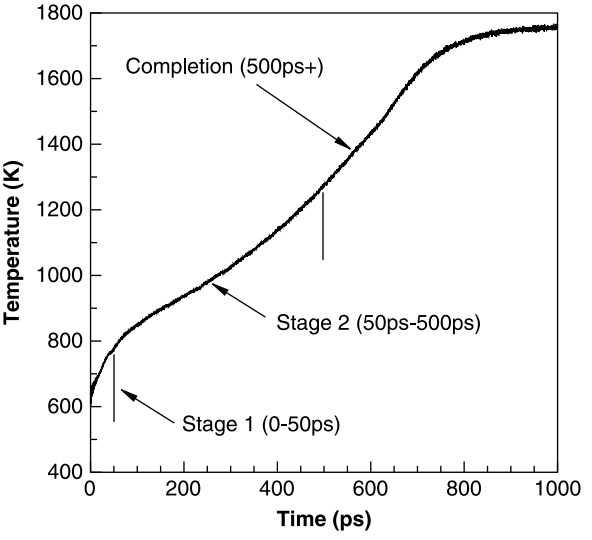

Figure 3. Time versus temperature plot for sintering of separate 10 nm diameter Al and Ni nanoparticles. The various stages of the coalescence processes are denoted on the curve, including the final completion stage that occurs after the Ni nanoparticle has melted.

nanoparticle coalescence stage and is governed by the material diffusion coefficients. Initially at stage 2 the Ni nanoparticle is still solid and the formation of Ni—Al bonds is only possible by Ni atoms on the surface of the core melting and diffusing away from the interface. This process proceeds until the Ni core has reached its melting point and mixing of the remaining Ni and Al atoms occurs more rapidly, driven by the enthalpy of formation of NiAl. From stage 2 until complete alloying has occurred, taking approximately 500 ps, the formation of Ni and Al bonds is the primary reaction driving force.

The transient system temperature results from the MD simulations are computed and shown in Figure 4. These results illustrate two important data points, first that the adiabatic temperature does indeed increase with decreasing nanoparticle size as predicted in the thermodynamic analysis and that the time to reach the adiabatic temperature increases with increasing nanoparticle size.

In Figure 4 it is apparent that the predicted adiabatic temperature from the thermodynamic analysis is in close agreement with the simulated temperature. Variability of the computed temperature arises from the wide range of experimental results for the surface tension for liquid Al and solid Ni, the reported enthalpy of formation for NiAl, and the assumed melting temperature for the Ni and NiAl materials at this scale. Each of these experimental data points are used in the thermodynamic analysis and contribute to the resulting small inaccuracies in the predicted temperature.

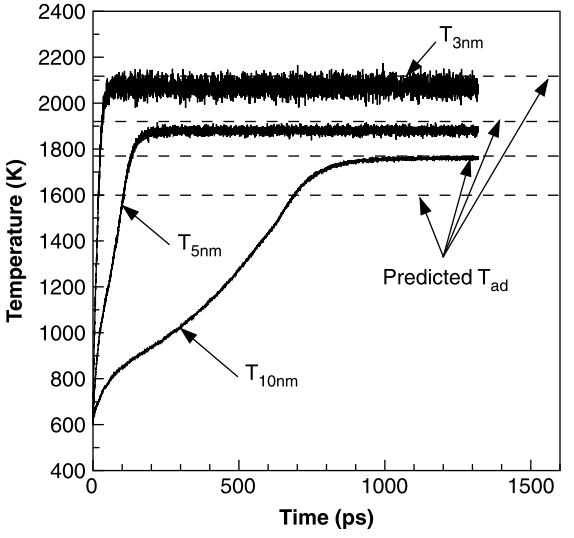

Figure 4. System temperature versus time in the sintering of nanoparticles with an Ni:Al ratio of 1:1. The subscripts in the legend refer to the diameter of the nanoparticle considered, i.e. 3, 5 and 10 nm. The dashed lines are the computed adiabatic temperature from the thermodynamic analysis. All of the dashed lines correspond reasonably well with the corresponding MD simulation results.

5.1 Sintering time

In addition to reaction temperature, we are also concerned with reaction time. In order to compute a characteristic reaction time for reactive synthesis we use the definition from Zhao et al. [31]. Zhao defines the reaction time as the time when the temperature has obtained 80% of the expected temperature increase, as defined in Equation (6)

$$T(t) = T_0 + 0.8(T_1 - T_0). \tag{6}$$

In Equation (6), T_0 is the initial temperature, T_1 is the maximum size dependent temperature reached, and $T(t)$ is the transient system temperature from the MD simulation. The reaction time is then computed by solving for t when the left and right hand sides of Equation (6) are equal. The computed size dependent reaction times imply that not only will the reaction temperature be higher, but will occur more rapidly with decreases in particle size. By analysis of the reaction time versus particle diameter we have determined that the reaction time scales to a power of approximately 2.5 versus particle diameter as shown in Figure 5. This is an interesting result because predicting a high rate of energy release is desirable for many applications. In addition, the value of the exponent indicates that surface area, which scales with the particle radius to a power of 2 and volume which scales with radius to a power of 3 both play important roles in the reaction time for nanoparticles in this size range.

5.2 Analysis of alloy formation

During the sintering of Ni and Al nanoparticles numerous local atomic ratios may be identified from the Ni–Al binary system[32–34]. The data presented here are

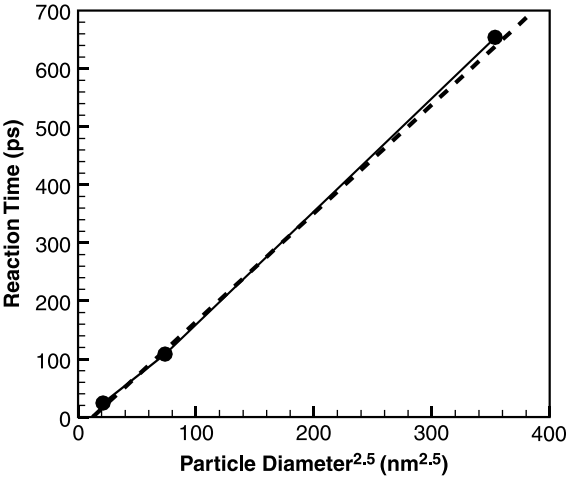

Figure 5. Reaction time versus Al nanoparticle diameter to a power of 2.5. Note the nearly linear relationship highlighted by the dashed line.

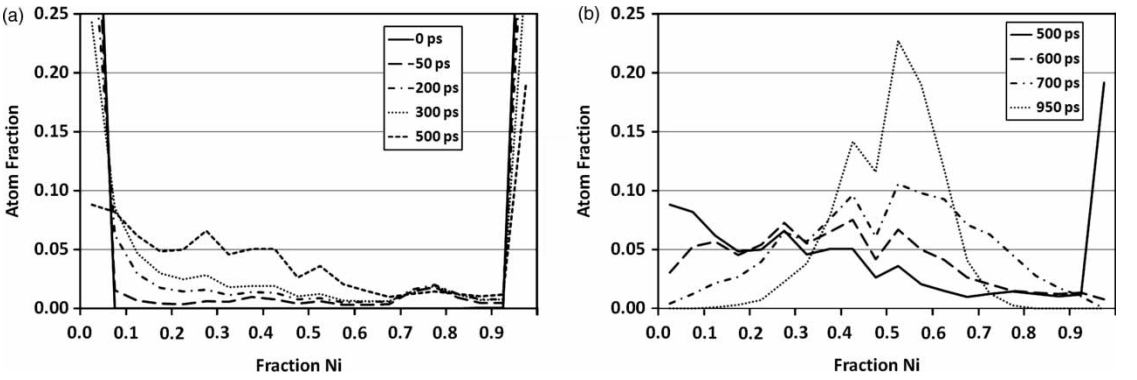

Figure 6. The results here show the fraction of Ni in each alloy versus fraction of all atoms in each alloy, i.e. a data point at (0.25, 0.1) corresponds to 10% of all atoms in the system belonging to Al_3Ni.

computed from the simulation results by calculating the local atomic ratios. These ratios are computed in order to analyze the spatial and temporal distribution of alloys in the simulation. The most commonly observed alloys for the Ni–Al binary system include Al_9Ni_2, Al_3Ni, Al_3Ni_2, NiAl, Ni_5Al_3, and Ni_3Al [33] corresponding to Ni fractions of 0.18, 0.25, 0.40, 0.50, 0.625, and 0.75, respectively. A comprehensive analysis of the measured atomic ratios in solution during sintering of separate nanoparticles is summarised here. Figure 6(a) and (b) show the normalised amount of computed solution ratios by Ni fraction through stage 2 and during stage 3, respectively.

During stage 1, from 0 to 50 ps for sintering of 10 nm diameter particles, most of the atoms remain in the pure metal phase, with only a small fraction of atoms, less than 5%, forming Ni-rich solutions such as Ni_3Al. In Figure 6(a) at 50 ps an observed peak at 0.75 fraction Ni (Ni_3Al) is likely due to the shorter bond length of Ni–Ni such that near the contact interface each Al atom will bond with multiple Ni atoms. During stage 2, the formation of Al-rich liquid solutions occurs at a rapid rate, quickly depleting the atomic fraction of pure Al in the system by the end of stage 2 (500 ps). In Figure 6(a) at 500 ps a small peak between 0.2 and 0.3 fraction Ni is observed, corresponding to Al_3Ni. At the end of stage 2 the largest portion of any material is still pure Ni, Figure 7(b). The initial formation of Al-rich solutions is supported by experimental observations [32,34]. The reaction process that produces these alloys is likely explained by Ni atoms diffusing into the liquid Al region forming Al-rich clusters of Al_3Ni. These clusters then diffuse through the Al melt, eventually forming the eutectic mixture. Figure 7(b) supports this process because small clusters of Al-rich alloys are clearly evident in the liquid Al, with some initial coalescence of clusters to obtain the eutectic atomic ratio.

The lines in Figure 6(b) for stage 3 indicate a rapid reduction in the amount of pure Ni and the corresponding formation of NiAl. During stages 1 and 2 as observed in Figure 3 the temperature of the system is rising monotonically. Near the start of stage 3 the system temperature has reached the melting point of Ni. At 700 ps, shortly after the Ni nanoparticle has completely melted, two peaks are present in Figure 6(b), near 40% Ni and 50%

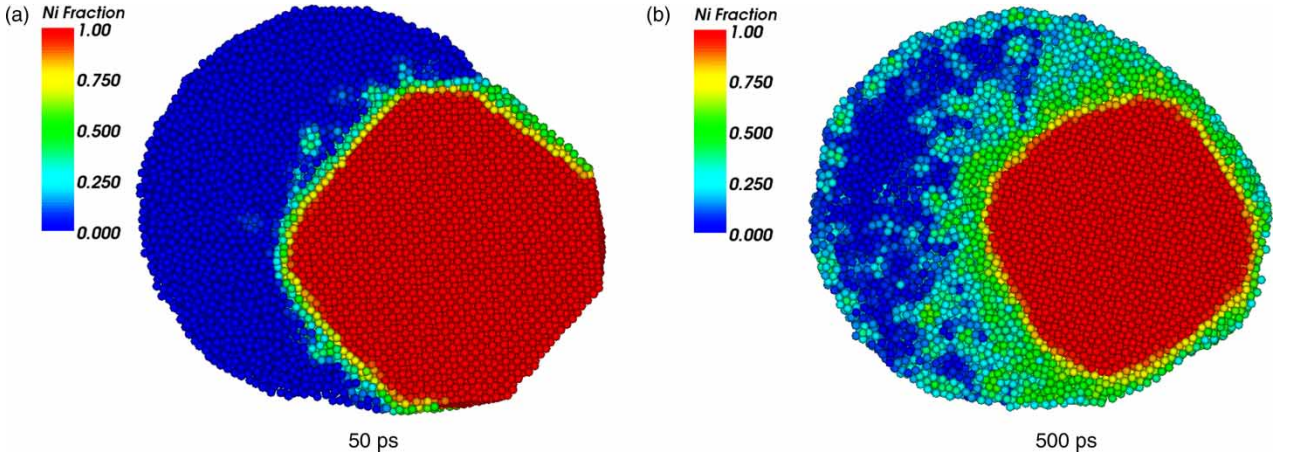

Figure 7. Plot showing spatial distribution of Ni fractions during stages 1 and 2 of the sintering process.

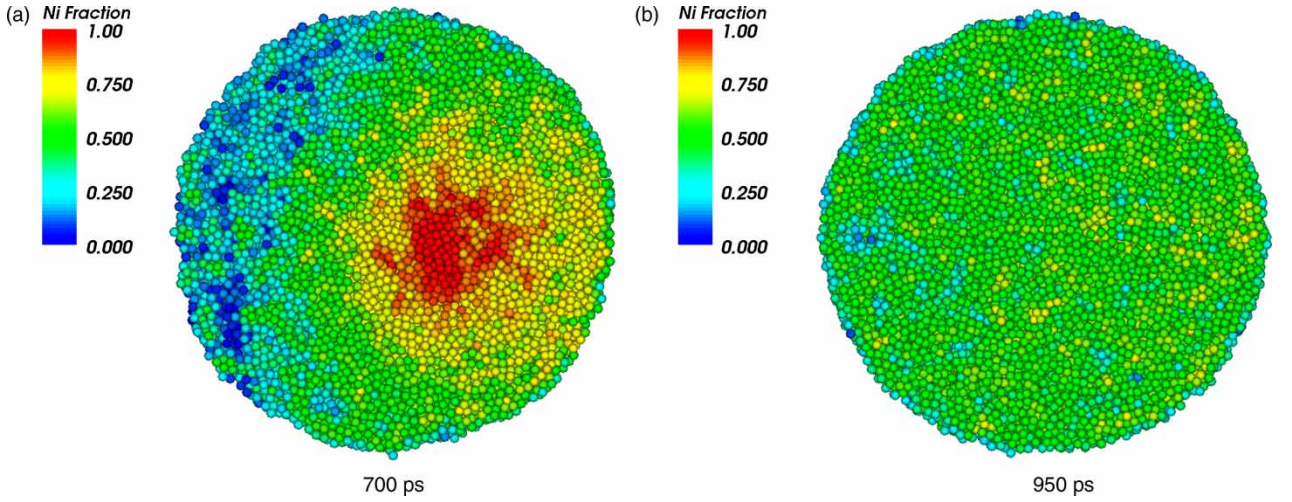

Figure 8. Plot showing spatial distribution of Ni fractions during stage 3 of the sintering process.

Ni, corresponding to Al_3Ni_2 and NiAl. In Figure 8(a), shortly after melting of the Ni nanoparticle, there is a Ni-rich region visible. This region quickly disappears as the SHS reaction proceeds rapidly to form the eutectic alloy. After nearly complete sintering at 950 ps, the majority of atoms are in a NiAl liquid solution with some temporal formation of other alloys. This brief analysis has demonstrated that the various solution ratios are an interesting problem that warrants closer thermodynamic analysis.

6. Conclusions

We have analysed a model system for the energetic reaction of Ni and Al nanoparticles. It was found that for the coalescing and sintering of separate nanoparticles the energy release from the change in surface area is only significant at small, less that 10 nm diameter, nanoparticles [24]. The MD simulations of nanoparticle sintering and thermodynamic analyses show that the reaction time will decrease and the adiabatic reaction temperature will increase with decreasing nanoparticle sizes. This has a potential to be an important issue for applications, where high energy release rates are desired. The simulation temperature data closely match a classical thermodynamic analysis performed here. The analysis of the alloys formed during sintering shows the initial formation of Al-rich compounds with Ni atoms diffusing from the Ni core into the Al melt. After the temperature has risen to the melting point of the Ni core a final eutectic alloy is formed. This final mixing and the associated temperature increase occurs very rapidly as indicated in the transient temperature result from the MD simulations and snapshots of the liquid solution near the end of stage 2.

Acknowledgements

The authors would like to acknowledge the support received by the U.S. Army Major Shared Resource Center (MSRC) at the Aberdeen Proving Ground, MD. Additional support was provided by the National Institute for Standards Technology (NIST) and the U.S. Army Research Office (ARO).

Note

1. Current address: School of Aerospace and Mechanical Engineering, The University of Oklahoma, Norman, OK, USA.

References

[1] X. Phung, J. Groza, E.A. Stach, L.N. Williams, and S.B. Ritchey, *Surface characterization of metal nanoparticles*, Mater. Sci. Eng. A 359 (2003), pp. 261–268.
[2] A. Rai, D. Lee, K. Park, and M.R. Zachariah, *Importance of phase change of aluminum in oxidation of aluminum nanoparticles*, J. Phys. Chem. B 108 (2004), pp. 14793–14795.
[3] H.P. Li, *Influence of ignition parameters on micropyretic synthesis of NiAl compound*, Mater. Sci. Eng. A 404 (2005), pp. 146–152.
[4] S. Gennari, U.A. Tamburini, F. Maglia, G. Spinolo, and Z.A. Munir, *A new approach to the modeling of SHS reactions: combustion synthesis of transition metal aluminides*, Acta Mater. 54 (2006), pp. 2343–2351.
[5] P. Nash and O. Kleppa, *Composition dependence of the enthalpies of formation of NiAl*, J. Alloys Compounds 321 (2001), pp. 228–231.
[6] R. Hu and P. Nash, *The enthalpy of formation of NiAl*, J. Mater. Sci. 40 (2005), pp. 1067–1069.
[7] J.C. Trenkle, T.P. Weihs, and T.C. Hufnagel, *Fracture toughness of bulk metallic glass welds made using nanostructured reactive multilayer foils*, Scr. Mater. 58 (2008), pp. 315–318.
[8] S. Dong, P. Hou, H. Cheng, H. Yang, and G. Zou, *Fabrication of intermetallic NiAl by self-propogating high-temperature synthesis reaction using aluminum nanopowder under high pressure*, J. Phys. Condensed Matter 14 (2002), pp. 11023–11030.
[9] L.J. Lewis, P. Jensen, and J.-L. Barrat, *Melting, freezing, and coalescence of gold nanoparticles*, Phys. Rev. B 56(4) (1997), pp. 2248–2257.
[10] T. Hawa and M.R. Zachariah, *Coalescence kinetics of bare and hydrogen-coated silicon nanoparticles: a molecular dynamics study*, Phys. Rev. B 71 (2005), 165434.

[11] T. Hawa and M.R. Zachariah, *Coalescence kinetics of unequal sized nanoparticles*, Aerosol Sci. 37 (2006), pp. 1–15.
[12] M.R. Zachariah and M.J. Carrier, *Molecular dynamics computation of gas-phase nanoparticle sintering: a comparison with phenomenological models*, J. Aerosol Sci. 30(9) (1999), pp. 1139–1151.
[13] S.H. Ehrman, *Effect of particle size on rate of coalescence of silica nanoparticles*, J. Colloid Interf. Sci. 213 (1999), pp. 258–261.
[14] S. Arcidiacono, N.R. Bieri, D. Poulikakos, and C.P. Grigoropoulos, *On the coalescence of gold nanoparticles*, Int. J. Multiphase Flow 30 (2004), pp. 979–994.
[15] S. Yu, C.-Y. Wang, T. Yu, and J. Cai, *Self-diffusion in the intermetallic compounds NiAl and Ni_3Al: an embedded atom method study*, Phys. B 396 (2007), pp. 138–144.
[16] Y. Mishin, M.J. Mehl, and D.A. Papaconstantopoulos, *Embedded-atom potential for B2-NiAl*, Phys. Rev. B 65 (2002), 224114.
[17] J. Mei, B.R. Cooper, and S.P. Lim, *Many-body atomistic model potential for intermetallic compounds and alloys and its application to NiAl*, Phys. Rev. B 54(1) (1996), pp. 178–183.
[18] F. Delogu, *Numerical simulation of the thermal response of Al core/Ni shell nanometer-sized particles*, Nanotechnology 18 (2007), 505702.
[19] H.X. Zhu and R. Abbaschian, *Reactive processing of nickel-aluminide intermetallic compounds*, J. Mater. Sci. 38 (2003), pp. 3861–3870.
[20] S.J. Plimpton, *Fast parallel algorithms for short-range molecular dynamics*, J. Comput. Phys. 117 (1995), pp. 1–19.
[21] M.W. Finnis and J.E. Sinclair, *A simple empirical N-body potential for transition metals*, Philos. Mag. A 50 (1984), pp. 45–55.
[22] J.E. Angelo, N.R. Moody, and M.I. Baskes, *Trapping of hydrogen to lattice defects in nickel*, Model. Simul. Mater. Sci. Eng. 3 (1995), pp. 289–307.
[23] G.J. Ackland and V. Vitek, *Many-body potentials and atomic-scale relaxations in noble-metal alloys*, Phys. Rev. B 41(15) (1990), pp. 10324–10333.
[24] B.J. Henz, T. Hawa, and M.R. Zachariah, *Molecular dynamics simulation of the kinetic reaction of Ni and Al Nanoparticles*, J. Appl. Phys., in press.
[25] P. Pawlow, Z Phys. Chem. 65 (1909), p. 545.
[26] P. Zhu, J.C.M. Li, and C.T. Liu, *Adiabatic temperature of combustion synthesis of Al–Ni systems*, Mater. Sci. Eng. A 357 (2003), pp. 248–257.
[27] M.R. Zachariah, M.J. Carrier, and E. Blasiten-Barojas, *Properties of silicon nanoparticles: a molecular dynamics study*, J. Phys. Chem. 100 (1996), pp. 14856–14864.
[28] A.Y. Lozovoĭ, K.V. Ponomarev, and Y.K. Vekilov, *First-principles investigation of thermal point defects in B2 NiAl*, Phys. Solid State 41(9) (1999), pp. 1494–1499.
[29] F.Z. Chrifi-Alaoui, M. Nassik, K. Mahdouk, and J.C. Gachon, *Enthalpies of formation of the Al–Ni intermetallic compounds*, J. Alloys Compounds 364 (2004), pp. 121–126.
[30] D. Mukherjee, C.G. Sonwane, and M.R. Zachariah, *Kinetic Monte-Carlo simulation of the effect of coalescence energy release on the size and shape evolution of nanoparticles grown as an aerosol*, J. Chem. Phys. 119 (2003), p. 3391.
[31] S. Zhao, T.C. Germann, and A. Strachan, *Atomistic simulations of shock-induced alloying reactions in Ni/Al nanolaminates*, J. Chem. Phys. 125 (2006), 164707.
[32] A. Kyriakopolous, M. Lynn, and R. Ghomashchi, *Reactive interaction of molten aluminum and solid nickel*, J. Mater. Sci. Lett. 20 (2001), pp. 1699–1701.
[33] S.O. Moussa and K. Morsi, *Reactive pressing of intermetallics*, Mater. Sci. Eng. A 454–455 (2007), pp. 641–647.
[34] X. Qiu and J. Wang, *Experimental evidence of two-stage formation of Al_3Ni in reactive Ni/Al multilayer foils*, Scr. Mater. 26 (2007), pp. 1055–1058.